Original Article

Longitudinal label-free optical-resolution photoacoustic microscopy of tumor angiogenesis *in vivo*

Riqiang Lin*, Jianhua Chen*, Huina Wang, Meng Yan, Wei Zheng, Liang Song

Research Laboratory for Biomedical Optics and Molecular Imaging, Shenzhen Key Laboratory for Molecular Imaging, Institute of Biomedical and Health Engineering, Shenzhen Institutes of Advanced Technology, Chinese Academy of Sciences, Shenzhen 518055, China

*These authors contributed equally to this work.

Correspondence to: Liang Song. Shenzhen Institutes of Advanced Technology, Chinese Academy of Sciences, 1068 Xueyuan Boulevard, Nanshan, Shenzhen 518055, China. Email: liang.song@siat.ac.cn.

Background: Optical-resolution photoacoustic microscopy (OR-PAM) is a high-resolution imaging technology capable of label-free imaging of the morphology and functions of the microvasculature *in vivo*. Previous studies of angiogenesis by OR-PAM were carried out primarily with transgenic mice and the mouse ear model. While important findings have been generated using this approach, the application of OR-PAM to the more widely used subcutaneous dorsal tumor models remains challenging, largely due to the respiratory and cardiac motion artifacts, as well as the protruding tumor contours.

Methods and materials: A noninvasive dorsal skin-fold (N-DSF) model, along with adaptive *z*-scanning and a corresponding experimental protocol, is developed. Mammary carcinoma cells (4T1) were administered subcutaneously to the backs of female BALB/c mice for tumor inoculation. The mice were anesthetized using a mixture of isofluorane and oxygen.

Results: *In vivo* OR-PAM of angiogenesis with subcutaneous dorsal tumor models in mice has been demonstrated. To test the performance of this method, we have monitored the growth of 4T1 mouse mammary carcinoma in BALB/c mice over a period of 9 days. The major features of tumor angiogenesis, including the change of vascular tortuosity, the dilation of vessel diameters, and the increase of blood supply, have been clearly captured with OR-PAM.

Conclusions: In combination with N-DSF model, OR-PAM has demonstrated outstanding capacity to provide label-free monitoring of angiogenesis in tumor. Thus, OR-PAM is of great potential to find broad biomedical applications in the pathophysiological studies of tumor and the treatments for anti-angiogenesis.

Keywords: Tumor angiogenesis; optical resolution photoacoustic microscopy (OR-PAM); dorsal skin-fold (DSF)

Submitted Oct 15, 2014. Accepted for publication Oct 21, 2014.
doi: 10.3978/j.issn.2223-4292.2014.11.08
View this article at: http://dx.doi.org/10.3978/j.issn.2223-4292.2014.11.08

Introduction

Angiogenesis is known to be a hallmark of malignant tumor growth, invasion, and metastasis (1,2). As early as in 1970s, a strategy that inhibits angiogenesis for anti-cancer therapy was proposed (3,4). Afterwards, in a few decades, investigations on angiogenesis have rapidly become one of the hottest topics in oncology research. Regulated by a number of growth factors secreted by tumor cells, the remodeling of existing vasculature and forming of new microvessels result in the alteration of the morphology of the microvascular networks (5). Clinical imaging modalities such as magnetic resonance imaging (MRI) and positron emission tomography (PET) have been applied to imaging tumor angiogenesis (6,7), but the lack of micrometer-level resolution limits their capacity to visualize fine feature changes in the microvasculature. In combination with a skin-fold window chamber mounted on a mouse's back or head, intravital microscopy (IVM) based on confocal or

two-photon laser scanning florescence microscope allows high-resolution imaging of tumors *in vivo* (8-12). However, due to the strong scattering of visible light in tissue, tissue penetration is usually a trade-off of the high resolution in IVM, which has an imaging depth of ~0.5 mm or less. To improve the imaging depth, optical frequency domain imaging (OFDI) and optical microangiography (OMAG) were developed and applied to imaging microvasculature networks (13-17). These techniques utilize near-infrared light to achieve a better imaging depth of ~1 mm, with sufficient spatial resolution (~10 μm) for visualizing most microvessels. In addition, they can be conveniently used for longitudinal imaging without the need of exogenous contrast agents, which are required for florescence-based IVM.

In recent decades, photoacoustic tomography (PAT) is rapidly emerging as a vital tool for many biomedical imaging applications (18). PAT is based on the detection and reconstruction of depth-resolved ultrasound waves induced by local absorption of short laser pulses in biological tissue. Due to the strong optical absorption of hemoglobin at visible and near-infrared wavelengths, PAT provides extremely high sensitivity for label-free imaging of the microvasculature *in vivo* (19). In addition, featured by significantly lower scattering of ultrasound in tissue compared to photons, PAT can offer a scalable imaging depth ranging from several millimeters to several centimeters, depending on the required spatial resolution (20). Previous studies using photoacoustic computed tomography (PA-CT) at low ultrasonic frequency successfully depicted the main trunks of the vascular network of subcutaneously implanted tumors on the mouse back (21-24). A Fabry-Perot polymer film ultrasound sensor was also applied for mapping the tumor vasculature with a spatial resolution of ~100 μm (25). However, to clearly visualize the finest microvessels (capillaries) in tumor angiogenesis, a spatial resolution of ~5 μm is required, which can be provided by optical-resolution photoacoustic microscopy (OR-PAM)—a technique that uses a tightly focused laser beam for photoacoustic excitation (26,27).

In order to avoid the respiratory and cardiac motion artifacts from living animals, previous studies of tumor angiogenesis by OR-PAM were carried out primarily on the ears of mice (28-30). Though impressive findings were generated, the ear is not commonly considered to be an ideal site for implanting tumors due to insufficient nutrition supply for tumor growth. A more widely used site for tumor implantation is the subcutaneous region on the back. In order to obtain sufficient optical imaging depth, conventionally, a skin-fold window chamber is mounted on the back of a mouse by surgical operation for imaging the tumor vasculature with IVM. In such a setup, the skin on the back of a mouse is stretched and fitted between two glass slides allowing *in vivo* optical microscopy. However, the skin-fold window chamber is invasive, and may disturb the microcirculation and microenvironment for tumor growth. In addition, the animals may become susceptible to infections, and thus make longitudinal studies more challenging. Finally, the glass slices of the chamber can attenuate the photoacoustic signals seriously due to the mismatch of acoustic impedance between the tissue and glass. Therefore, it is essential to design a new experimental protocol with auxiliary devices dedicated to OR-PAM for angiogenesis imaging. In this study, a novel noninvasive dorsal skin-fold (N-DSF) animal fixture, together with adaptive *z*-scanning and a corresponding experimental protocol, is developed, which, for the first time to our knowledge, has enabled *in vivo*. OR-PAM of subcutaneously implanted tumors in the dorsal region of mice.

Methods and materials

Imaging system setup

A detailed description of our OR-PAM system can be found in our previous publications (31,32). Briefly, as illustrated in *Figure 1*, a 1.8-ns pulsed laser beam emitted at 532 nm from an Nd:YAG laser source (SPOT-532, Elforlight, UK) was focused to an optical diffraction-limited spot to irradiate the sample for excitation. Then, a 75-MHz transducer (V2022, Olympus-NDT, Japan) was used to detect the time-resolved photoacoustic signals from the sample. A-line pulse repetition rate of up to 5 kHz was used in all experiments. The motor scanning and data acquisition (DAQ) were controlled by customized computer software written in LabView (2011, National Instruments). A volumetric dataset could be obtained by two-dimensional mechanical scanning of the imaging probe. Using the photoacoustic signals from the tumor skin surface as feedback, the height of the imaging probe was adjusted adaptively during the acquisition of successive B-scans. This adaptive scanning was helpful for enabling the major tumor microvessels to be imaged within focus, although their height may vary due to the protruding tumor contour.

Animal tumor model

Female BALB/c mice (4-6 weeks old and weighted 18-20 g)

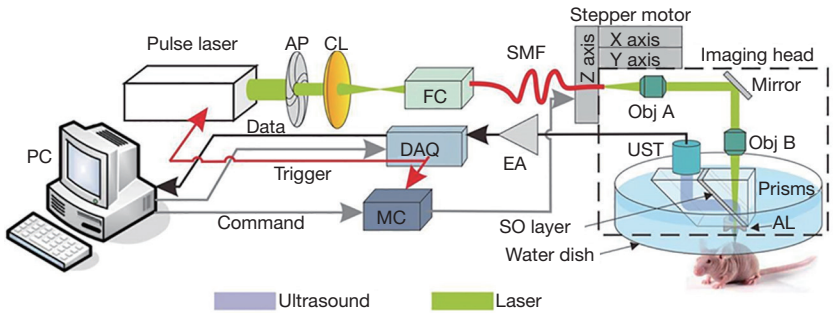

Figure 1 Schematic of the OR-PAM system. AP, aperture; CL, convex lens; FC, fiber coupler; SMF, single mode fiber; Obj, objective; UST, ultrasonic transducer; AL, acoustic lens; SO, silicone oil; EA, electrical amplifier; DAQ, data acquisition; PC, personal computer; OR-PAM, optical-resolution photoacoustic microscopy.

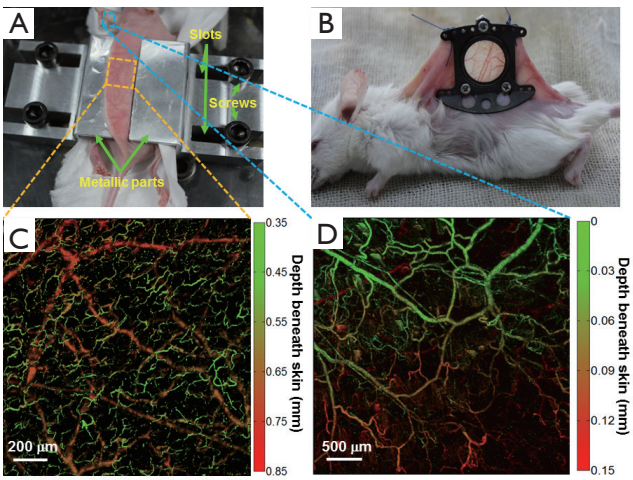

Figure 2 (A) N-DSF mouse fixture designed for our OR-PAM system. The dorsal skin only needs to be slightly clamped temporarily using this fixture; (B) Traditional invasive skin-fold window chamber used for intravital optical microscopy, permanently mounted on the mouse back by a surgical operation; (C) a representative depth-encoded MAP image of a normal mouse's dorsal region acquired by the combined use of OR-PAM and N-DSF fixture; (D) a representative depth-encoded MAP image of a normal mouse ear acquired by OR-PAM. The color scale represents depth below the skin surface. N-DSF, noninvasive dorsal skin-fold; OR-PAM, optical-resolution photoacoustic microscopy; MAP, maximum amplitude projection.

were purchased from the Medical Experimental Animal Center of Guangdong Province (Guangzhou, China). Mouse 4T1 mammary carcinoma cells were cultured with DMEM. The culture media were supplemented with 10% fetal bovine serum and 1% antibiotics-antimycotics. For tumor inoculation, cells (1×10^6 cells/mouse) were suspended in serum-free DMEM medium and administered subcutaneously to the backs of the mice.

Imaging procedure

All experimental animal procedures were carried out in compliance with protocols approved by the Animal Studies Committee of the Shenzhen Institutes of Advanced Technology, the Chinese Academy of Sciences. The mice were anesthetized using a mixture of isofluorane and oxygen at a concentration of 4% isofluorane for induction and 1.5% for maintenance (flow rate: 300 mL/min). The implanted tumor was positioned at the center of the scanning region. Acoustic gel was smeared between the skin and water tank for ultrasound coupling. Typically, one imaging session for a scanning region of 6 mm × 8 mm was completed within ~40 min. The tumors were imaged every 2 or 3 days after implantation. In all *in vivo* experiments, the optical energy fluence was maintained around 18 mJ/cm^2 on the skin surface, which conforms to the ANSI standard (ANSI Z136.3-2005).

N-DSF mouse fixture

The overall architecture of the N-DSF fixture is shown in *Figure 2A*. The dorsal skin was gently lifted up and flattened on the top surface of the fixture. The relative positions of the two symmetrical metallic parts of the fixture can be adjusted via a pair of parallel slots to slightly clamp the skin. Then, four screws were used to fasten the entire fixture onto the platform.

Compared with skin-fold window chamber as shown in *Figure 2B*, our new fixture is noninvasive, which is quite

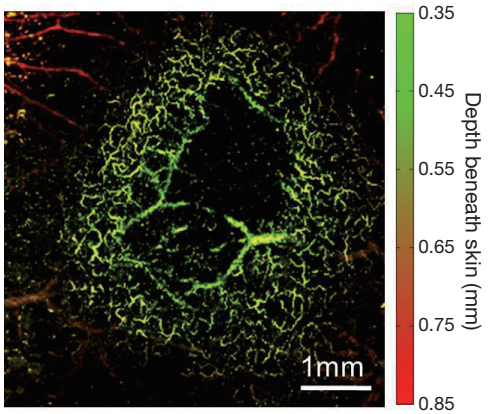

Figure 3 Photoacoustic depth-encoded MAP of a subcutaneously implanted 4T1 mouse mammary carcinoma 4 days after implantation. MAP, maximum amplitude projection.

beneficial for long-term imaging of tumor angiogenesis *in vivo*. In *Figure 2C*, a depth-encoded maximum amplitude projection (MAP) image of the subcutaneous blood vessels of a normal mouse is shown. In the image, different depths were encoded by various colors from green (superficial) to red (deep). From *Figure 2C,D*, it can be seen that the vascular morphologies of the ear and back are quite different. In particular, in *Figure 2C*, two distinct layers of vessels are shown, with the upper layer representing capillary-level microvessels in the dermis, while the lower layer representing relatively large arteries and veins beneath the dermis. The results suggest that our N-DSF mouse fixture is an effective tool dedicated to OR-PAM for imaging subcutaneous vessels.

Results

Using OR-PAM, first, we demonstrated an example of imaging 4T1 mouse mammary tumor (day 4 post implantation), as shown in *Figure 3*. The tumor was located at the center of the image, surrounded by a dense vascular network of the dorsal skin; several feeding vessels beneath and within the tumor could also be visualized. The dark region in the center of the image might be attributed to the necrosis of the tumor core. Overall, it can be seen that the high lateral resolution of OR-PAM has offered a unique capacity to clearly identify the surrounding tumor vasculature without any exogenous contrast agent.

Further, a series of longitudinal images of the developing 4T1 tumor angiogenesis was acquired every 2 to 3 days. Representative images acquired on days 5, 7, and 9 are shown in *Figure 4*, exhibiting the progressive growth of the tumor vessels. Quantitative analyses of selected representative vessels and regions were shown in *Figure 5*. *Figure 5A* compares the cross-sectional diameters averaged over 10 evenly selected positions along the vessel indicated by the green arrow in *Figure 4*. The error bars in the graph represent the standard deviations of the diameters measured at different positions. It shows that the average diameter of the vessel has increased by ~70.9% over 4 days. *Figure 5B* lists the integrated photoacoustic signals in the areas marked by the dashed white circles in *Figure 4*, revealing a >1.5-fold increase of blood flow in the tumor surrounding vessels. Accordingly, to show the depth of different vessels, the depth-encoded MAPs are also shown in *Figure 4*, where signals from superficial vessels are in green while signals from deeper ones are in red.

Figure 6 shows another series of longitudinal OR-PAM of 4T1 mouse tumor angiogenesis. Similar to the previous case, the results in *Figure 6A-C* are featured by gradually chaotic vasculature network, and an increased tortuosity of the vasculature surrounding the tumor. The remodeling of vasculature along tumor growth is further identified in *Figure 6*, as shown by the arrows pointing to several representative vessels. In *Figure 6*, each representative vessel is labeled by one arrow of a fixed color.

Conclusions

To the best of our knowledge, this work represents the first demonstration of longitudinal OR-PAM of angiogenesis in a subcutaneous dorsal tumor model in mouse. It shows that, by utilizing a newly-designed N-DSF fixture, our OR-PAM system provides an outstanding capacity in label-free monitoring of developing angiogenic vasculature. Various morphological changes of tumor vasculature were clearly visualized at high resolution. Specifically, the dynamics of tumor vascular density, diameter, and tortuosity were quantitatively tracked and analyzed over several days. Also, it can be seen that, although the same tumor cell line (4T1) was used in two series of experiments, the tumor vascular morphology could be distinct, as a result of the animal individual differences. However, some common features, including the increase of vascular density and tortuosity, were still observed. The results suggest that, OR-PAM system is of great potential to find broad biomedical applications related to revealing the pathophysiology of tumor, and the monitoring of anti-

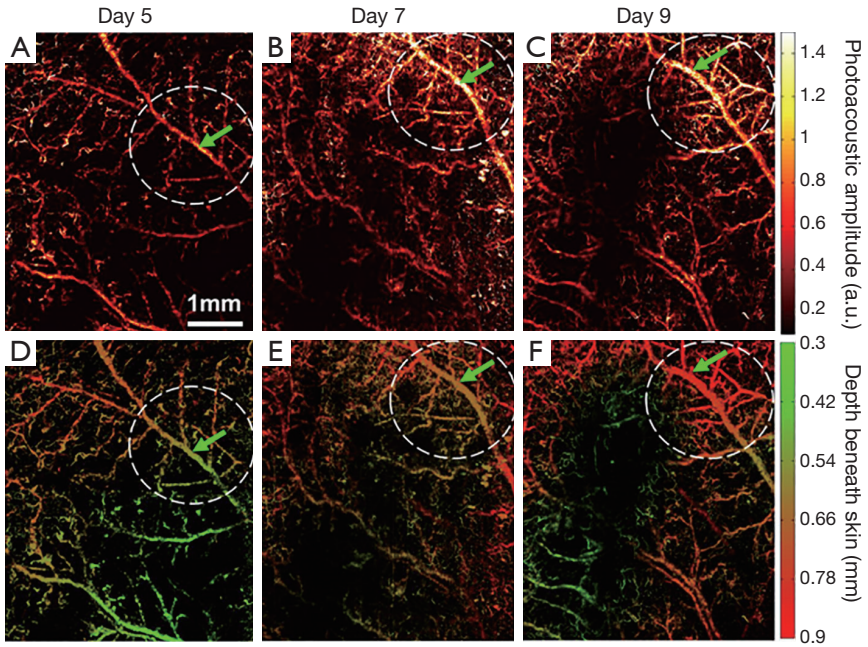

Figure 4 Longitudinal OR-PAM of developing 4T1 tumor angiogenesis (case 1) on (A) day 5; (B) day 7; and (C) day 9 post implantation; (D-F) depth-encoded MAP corresponding to (A-C). The vessel indicated by the green arrow and the region marked by the white dashed circle are extracted for further quantitative analysis shown in *Figure 5*. OR-PAM, optical-resolution photoacoustic microscopy; MAP, maximum amplitude projection.

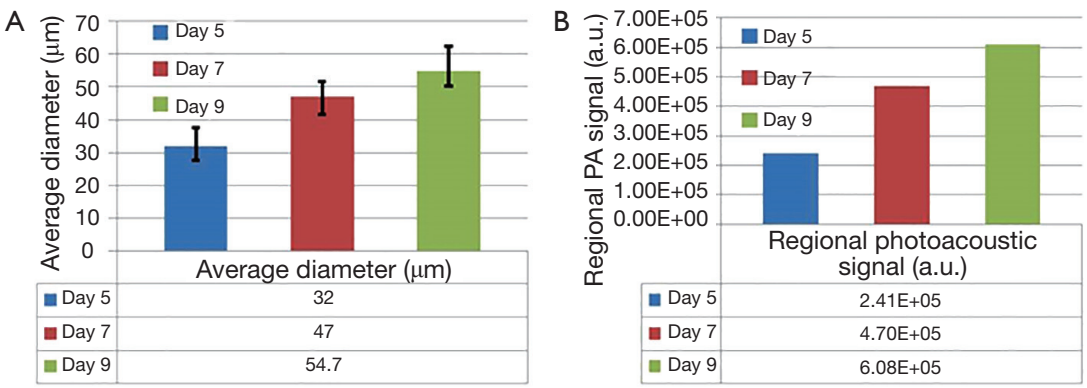

Figure 5 (A) Diameter change of the vessel indicated by the green arrow in *Figure 4*. The values are calculated by averaging over 10 evenly selected locations along the vessel. The error bar represents the standard deviation of the 10 measurements. (B) Change of the photoacoustic signals integrated over the area marked by the dashed white circle in *Figure 4*.

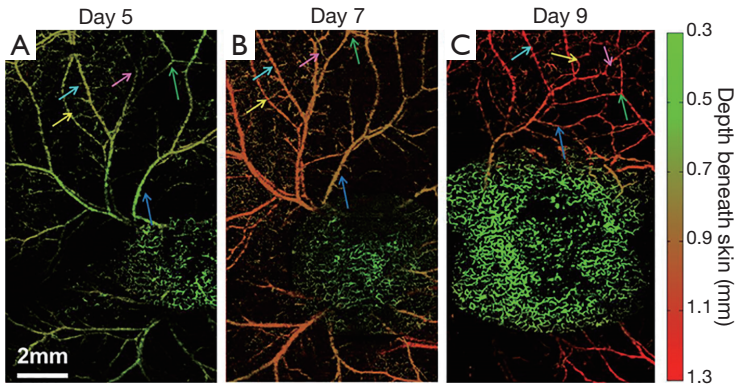

Figure 6 Longitudinal OR-PAM of developing 4T1 tumor angiogenesis (case 2) on (A) day 5; (B) day 7; and (C) day 9 post implantation. Obvious vascular morphology changes can be identified by examining each representative vessel labeled by a colored arrow. OR-PAM, optical-resolution photoacoustic microscopy.

angiogenesis treatments.

Acknowledgements

This work was supported in part by the National Natural Science Foundation of China grant: 61205203, 81427804, 61405234, and 61475182; the National Key Basic Research [973] Program of China: 2014CB744503, and 2015CB755500; the Shenzhen Science and Technology Innovation Committee grants: ZDSY-2013-0401165820-357, KQCX-2012-0816155844-962, CXZZ-2012-0617113635-699, and JCYJ-2012-0615125857-842; Guangdong Innovation Research Team Fund for Low-cost Healthcare Technologies (GIRTF-LCHT).

Disclosure: The authors declare no conflict of interests.

References

1. Weis SM, Cheresh DA. Tumor angiogenesis: molecular pathways and therapeutic targets. Nat Med 2011;17:1359-70.
2. Carmeliet P, Jain RK. Molecular mechanisms and clinical applications of angiogenesis. Nature 2011;473:298-307.
3. Folkman J. Anti-angiogenesis: new concept for therapy of solid tumors. Ann Surg 1972;175:409-16.
4. Brem H, Folkman J. Inhibition of tumor angiogenesis mediated by cartilage. J Exp Med 1975;141:427-39.
5. Albini A, Tosetti F, Li VW, Noonan DM, Li WW. Cancer prevention by targeting angiogenesis. Nat Rev Clin Oncol 2012;9:498-509.
6. Emblem KE, Mouridsen K, Bjornerud A, Farrar CT, Jennings D, Borra RJ, Wen PY, Ivy P, Batchelor TT, Rosen BR, Jain RK, Sorensen AG. Vessel architectural imaging identifies cancer patient responders to anti-angiogenic therapy. Nat Med 2013;19:1178-83.
7. Haubner R, Beer AJ, Wang H, Chen X. Positron emission tomography tracers for imaging angiogenesis. Eur J Nucl Med Mol Imaging 2010;37:S86-103.
8. Padera TP, Stoll BR, So PT, Jain RK. Conventional and high-speed intravital multiphoton laser scanning microscopy of microvasculature, lymphatics, and leukocyte-endothelial interactions. Mol Imaging 2002;1:9-15.
9. Jain RK, Munn LL, Fukumura D. Dissecting tumour pathophysiology using intravital microscopy. Nat Rev Cancer 2002;2:266-76.
10. Fukumura D, Duda DG, Munn LL, Jain RK. Tumor microvasculature and microenvironment: novel insights through intravital imaging in pre-clinical models. Microcirculation 2010;17:206-25.
11. Hak S, Reitan NK, Haraldseth O, de Lange Davies C. Intravital microscopy in window chambers: a unique tool to study tumor angiogenesis and delivery of nanoparticles. Angiogenesis 2010;13:113-30.
12. Koehl GE, Gaumann A, Geissler EK. Intravital microscopy of tumor angiogenesis and regression in the dorsal skin fold chamber: mechanistic insights and preclinical testing of therapeutic strategies. Clin Exp Metastasis 2009;26:329-44.
13. Vakoc BJ, Lanning RM, Tyrrell JA, Padera TP, Bartlett LA, Stylianopoulos T, Munn LL, Tearney GJ, Fukumura

D, Jain RK, Bouma BE. Three-dimensional microscopy of the tumor microenvironment in vivo using optical frequency domain imaging. Nat Med 2009;15:1219-23.
14. Vakoc BJ, Fukumura D, Jain RK, Bouma BE. Cancer imaging by optical coherence tomography: preclinical progress and clinical potential. Nat Rev Cancer 2012;12:363-8.
15. Wang RK, An L. Doppler optical micro-angiography for volumetric imaging of vascular perfusion in vivo. Opt Express 2009;17:8926-40.
16. Wang RK, An L, Francis P, Wilson DJ. Depth-resolved imaging of capillary networks in retina and choroid using ultrahigh sensitive optical microangiography. Opt Lett 2010;35:1467-9.
17. Reif R, Wang RK. Label-free imaging of blood vessel morphology with capillary resolution using optical microangiography. Quant Imaging Med Surg 2012;2:207-12.
18. Wang LV, Hu S. Photoacoustic tomography: in vivo imaging from organelles to organs. Science 2012;335:1458-62.
19. Hu S, Wang LV. Photoacoustic imaging and characterization of the microvasculature. J Biomed Opt 2010;15:011101.
20. Wang LV. Prospects of photoacoustic tomography. Med Phys 2008;35:5758-67.
21. Lao Y, Xing D, Yang S, Xiang L. Noninvasive photoacoustic imaging of the developing vasculature during early tumor growth. Phys Med Biol 2008;53:4203-12.
22. Lungu GF, Li ML, Xie X, Wang LV, Stoica G. In vivo imaging and characterization of hypoxia-induced neovascularization and tumor invasion. Int J Oncol 2007;30:45-54.
23. Ku G, Wang X, Xie X, Stoica G, Wang LV. Imaging of tumor angiogenesis in rat brains in vivo by photoacoustic tomography. Appl Opt 2005;44:770-5.
24. Siphanto RI, Thumma KK, Kolkman RG, van Leeuwen TG, de Mul FF, van Neck JW, van Adrichem LN, Steenbergen W. Serial noninvasive photoacoustic imaging of neovascularization in tumor angiogenesis. Opt Express 2005;13:89-95.
25. Laufer J, Johnson P, Zhang E, Treeby B, Cox B, Pedley B, Beard P. In vivo preclinical photoacoustic imaging of tumor vasculature development and therapy. J Biomed Opt 2012;17:056016.
26. Maslov K, Zhang HF, Hu S, Wang LV. Optical-resolution photoacoustic microscopy for in vivo imaging of single capillaries. Opt Lett 2008;33:929-31.
27. Rao B, Li L, Maslov K, Wang L. Hybrid-scanning optical-resolution photoacoustic microscopy for in vivo vasculature imaging. Opt Lett 2010;35:1521-3.
28. Oladipupo S, Hu S, Kovalski J, Yao J, Santeford A, Sohn RE, Shohet R, Maslov K, Wang LV, Arbeit JM. VEGF is essential for hypoxia-inducible factor-mediated neovascularization but dispensable for endothelial sprouting. Proc Natl Acad Sci U S A 2011;108:13264-9.
29. Oladipupo SS, Hu S, Santeford AC, Yao J, Kovalski JR, Shohet RV, Maslov K, Wang LV, Arbeit JM. Conditional HIF-1 induction produces multistage neovascularization with stage-specific sensitivity to VEGFR inhibitors and myeloid cell independence. Blood 2011;117:4142-53.
30. Hu S, Maslov K, Wang LV. In vivo functional chronic imaging of a small animal model using optical-resolution photoacoustic microscopy. Med Phys 2009;36:2320-3.
31. Chen J, Lin R, Wang H, Meng J, Zheng H, Song L. Blind-deconvolution optical-resolution photoacoustic microscopy in vivo. Opt Express 2013;21:7316-27.
32. Yang Z, Chen J, Yao J, Lin R, Meng J, Liu C, Yang J, Li X, Wang L, Song L. Multi-parametric quantitative microvascular imaging with optical-resolution photoacoustic microscopy in vivo. Opt Express 2014;22:1500-11.

Cite this article as: Lin R, Chen J, Wang H, Yan M, Zheng W, Song L. Longitudinal label-free optical-resolution photoacoustic microscopy of tumor angiogenesis *in vivo*. Quant Imaging Med Surg 2015;5(1):23-29. doi: 10.3978/j.issn.2223-4292.2014.11.08

